J|A|C|S
ARTICLES
Published on Web 02/13/2003

Highly Efficient Water Splitting into H_2 and O_2 over Lanthanum-Doped $NaTaO_3$ Photocatalysts with High Crystallinity and Surface Nanostructure

Hideki Kato,[†] Kiyotaka Asakura,[‡] and Akihiko Kudo*,[†]

Contribution from the Department of Applied Chemistry, Faculty of Science, Science University of Tokyo, 1-3 Kagurazaka, Shinjuku-ku, Tokyo 162-8601, Japan and Catalysis Research Center, Hokkaido University, 11 Kita 10 Nishi, Kita-ku, Sapporo 060-0811, Japan

Received July 18, 2002; E-mail: a-kudo@rs.kagu.tus.ac.jp

Abstract: NiO-loaded $NaTaO_3$ doped with lanthanum showed a high photocatalytic activity for water splitting into H_2 and O_2 in a stoichiometric amount under UV irradiation. The photocatalytic activity of NiO-loaded $NaTaO_3$ doped with lanthanum was 9 times higher than that of nondoped NiO-loaded $NaTaO_3$. The maximum apparent quantum yield of the NiO/$NaTaO_3$:La photocatalyst was 56% at 270 nm. The factors affecting the highly efficient photocatalytic water splitting were examined by using various characterization techniques. Electron microscope observations revealed that the particle sizes of $NaTaO_3$:La crystals (0.1−0.7 μm) were smaller than that of the nondoped $NaTaO_3$ crystal (2−3 μm) and that the ordered surface nanostructure with many characteristic steps was created by the lanthanum doping. The small particle size with a high crystallinity was advantageous to an increase in the probability of the reaction of photogenerated electrons and holes with water molecules toward the recombination. Transmission electron microscope observations and extended X-ray absorption fine structure analyses indicated that NiO cocatalysts were loaded on the edge of the nanostep structure of $NaTaO_3$:La photocatalysts as ultrafine particles. The H_2 evolution proceeded on the ultrafine NiO particles loaded on the edge while the O_2 evolution occurred at the groove of the nanostep structure. Thus, the reaction sites for H_2 evolution were separated from those of O_2 evolution over the ordered nanostep structure. The small particle size and the ordered surface nanostep structure of the NiO/$NaTaO_3$:La photocatalyst powder contributed to the highly efficient water splitting into H_2 and O_2.

Introduction

Photocatalytic water splitting into H_2 and O_2 is an important reaction from a viewpoint of the photon energy conversion. The water splitting to produce H_2 and O_2 is an uphill reaction with a large positive change in the Gibbs free energy (237 kJ mol^{-1}). It is necessary for water splitting by semiconductor photocatalysts that their conduction band levels are more negative than the reduction potential of H_2O to produce H_2 and their valence band levels are more positive than the oxidation potential of H_2O to produce O_2. However, such a term of band potentials is just one of the requirements concerned with thermodynamics. Other important factors are concerned with photocatalytic water splitting.[1] Efficient charge separation and suppression of recombination between photogenerated electrons and holes are important factors for efficient photocatalytic water splitting. Moreover, creation and separation of active sites for H_2 and O_2 evolution are also important. Loading of cocatalysts such as Pt and NiO is necessary for many photocatalyst materials to introduce the active sites for H_2 formation. For water splitting which is an uphill reaction, it is especially important to avoid the back reaction between H_2 and O_2 and their intermediates to form H_2O.

Some oxides which are active photocatalysts for water splitting under UV light irradiation, such as TiO_2,[2−4] $SrTiO_3$,[5,6] $K_4Nb_6O_{17}$,[7] $Na_2Ti_6O_{13}$,[8a] $BaTi_4O_9$,[8b] ZrO_2,[9a] Ta_2O_5,[9b] $K_2La_2Ti_3O_{10}$,[10] $Sr_2Nb_2O_7$,[11,12] and $ZnNb_2O_6$,[13] possess the nature satisfying the factors mentioned above. In particular, $K_4Nb_6O_{17}$ and $K_2La_2Ti_3O_{10}$ with layered structures showed high activities. The layered structures avail for the separation of the reaction site for H_2 and O_2 evolution to avoid the back reaction. It is no good that H_2 evolution sites are too close to O_2 evolution sites

* Address correspondence to this author. Fax: +81-33235-2214.
[†] Science University of Tokyo.
[‡] Hokkaido University.

(1) Kudo, A. *J. Ceram. Soc. Jpn.* **2001**, *109*, S81−S88.
(2) Yamaguchi, K.; Sato, S. *J. Chem. Soc., Faraday Trans. 1* **1985**, *81*, 1237−1246.
(3) Kudo, A.; Domen, K.; Maruya, K.; Onishi, T. *Chem. Phys. Lett.* **1987**, *133*, 517−519.
(4) Sayama, K.; Arakawa, H. *J. Chem. Soc., Faraday Trans.* **1997**, *93*, 1647−1654.
(5) Lehn, J.-M.; Sauvage, J.-P.; Ziessel, R. *Nouv. J. Chim.* **1980**, *4*, 623−627.
(6) (a) Domen, K.; Kudo, A.; Onishi, T.; Kosugi, N.; Kuroda, H. *J. Phys. Chem.* **1986**, *90*, 292−295. (b) Domen, K.; Kudo, A.; Onishi, T. *J. Catal.* **1986**, *102*, 92−98.
(7) Kudo, A.; Sayama, K.; Tanaka, A.; Asakura, K.; Domen, K.; Maruya, K.; Onishi, T. *J. Catal.* **1989**, *120*, 337−352.
(8) (a) Inoue, Y.; Ogura, S.; Kohno, M.; Sato, K. *Appl. Surf. Sci.* **1997**, *121/122*, 521−524. (b) Inoue, Y.; Kohno, M.; Kaneko, T.; Ogura, S.; Sato, K. *J. Chem. Soc., Faraday Trans.* **1998**, *94*, 89−94.
(9) (a) Sayama, K.; Arakawa, H. *J. Phys. Chem.* **1993**, *97*, 531−533. (b) Sayama, K.; Arakawa, H. *J. Photochem. Photobiol., A* **1994**, *77*, 243−247.
(10) Takata, T.; Shinohara, K.; Tanaka, A.; Hara, M.; Kondo, J. N.; Domen, K. *J. Photochem. Photobiol., A* **1997**, *106*, 45−49.
(11) Kim, H. G.; Hwang, D. W.; Kim, J.; Kim, Y. G.; Lee, J. S. *Chem. Commun.* **1999**, 1077−1078.
(12) Kudo, A.; Kato, H.; Nakagawa, S. *J. Phys. Chem. B* **2000**, *104*, 571−575.
(13) Kudo, A.; Nakagawa, S.; Kato, H. *Chem. Lett.* **1999**, 1197−1198.

10.1021/ja027751g CCC: $25.00

on a photocatalyst surface. It seems to be advantageous that their evolution sites are separated from each other in nanometer scale to avoid the back reaction. Therefore, constructing the characteristic surface nanostructure will be useful for the design of the separated active sites to develop highly active photocatalysts for water splitting.

Recently, the authors and other groups have reported that many tantalates, $K_3Ta_3Si_2O_{13}$,[14a] alkali tantalates $ATaO_3$ (A: Li, Na, and K),[14e] alkaline earth tantalates $A'Ta_2O_6$ (A′: Ca, Sr, and Ba),[14b, c] $Sr_2Ta_2O_7$,[12,14f] $KLn_2Ta_5O_{15}$,[14d] $KTaO_3$ doped with Zr or Hf,[15] and $RbNbTa_2O_7$,[16] show high activities for photocatalytic water splitting under UV light irradiation. In particular, $NaTaO_3$ with a perovskite structure is most active among tantalates. However, the $NaTaO_3$ photocatalyst was deactivated with the reaction time. It is important to suppress the deactivation and improve the photocatalytic activity. Recently, the authors have preliminarily reported that the activity of the NiO/$NaTaO_3$ photocatalyst is drastically improved by lanthanide doping into the $NaTaO_3$ crystals.[17] Therefore, it is important to clarify the effect of the doping on the improvement of photocatalytic properties to obtain information for the design of photocatalysts.

In the present study, photocatalytic water splitting over NiO/$NaTaO_3$ doped with lanthanum was investigated. Photocatalysts were characterized by X-ray diffraction, diffuse reflection spectroscopy, electron microscopy, and extended X-ray absorption fine structure analyses to clarify the mechanism for highly efficient water splitting. The role of the surface nanostructure created by the lanthanum doping was also discussed.

Experimental Section

Preparation of Lanthanum-Doped $NaTaO_3$ Photocatalysts. Lanthanum-doped $NaTaO_3$ powder (denoted as $NaTaO_3$:La hereafter) was prepared by a solid-state reaction. The starting materials, La_2O_3 (Wako Pure Chemical; 99.99%), Na_2CO_3 (Kanto Chemical; 99.5%), and Ta_2O_5 (Rare Metallic; 99.99%), were mixed according to the ratio Na:La:Ta = 1−X:X:1 supposing that the sodium ions were replaced by lanthanum ions. The excess amount of sodium (5 mol %) was added in the mixture to compensate the volatilization. The mixture was calcined in air at 1170 K for 1 h and 1420 K for 10 h with intermediate grinding using a platinum crucible and a muffle furnace. The excess sodium was washed out with water after calcination. Seven grams of the calcined powder was dispersed in 50 mL of water and stirred at room temperature for 10 min. After filtration, the powder was dried at 320 K for 2−12 h in air. The obtained powder was confirmed by X-ray diffraction using Cu Kα radiation (Rigaku; RINT-1400). A NiO cocatalyst was loaded by an impregnation method from an aqueous solution of $Ni(NO_3)_2 \cdot 6H_2O$ (Wako Pure Chemical; 98.0%). One and one-tenth grams of the $NaTaO_3$:La powder and a small amount of water (ca. 1 mL) containing the appropriate amount of $Ni(NO_3)_2 \cdot 6H_2O$ were put into a porcelain crucible. Water was evaporated on a water bath. The suspension was stirred using a glass rod during the evaporation. The dried powder was calcined at 540 K for 1 h in air using a muffle furnace. A Pt cocatalyst was loaded by a photodeposition method from an aqueous solution of $H_2PtCl_6 \cdot 6H_2O$ (Tanaka Kikinnzoku; 37.47% as Pt).

Photocatalytic Reactions. Photocatalytic reactions were carried out in a gas-closed circulation system with 1690 mL of the dead volume. The photocatalyst powder (1 g) was dispersed in a reactant solution (390 mL) by a magnetic stirrer in an inner irradiation cell made of quartz. Pure water and aqueous solutions of methanol and silver nitrate were employed as reactant solutions for water splitting into H_2 and O_2, H_2 evolution, and O_2 evolution, respectively. In some cases, NaOH was added to control the pH of the solution. The light source was a 400 W high-pressure mercury lamp (SEN; HL400EH-5). The amounts of H_2 and O_2 evolved were determined using gas chromatography (Shimadzu; GC-8A, MS-5A column, TCD, Ar carrier) or by volumetric measurement.

Apparent quantum yields were measured using a reaction cell with top window made of quartz and a 300 W Xe illuminator (ILC technology; CERMAX-LX300) attached with a band-pass filter (Kenko; BPUV-270, WHM: 16 nm).[14e] The photocatalyst powder (0.05−0.5 g) was dispersed in pure water (300 mL) for the determination of the apparent quantum yields.

$$\text{apparent quantum yield (\%)} = \{(\text{the number of reacted electrons})/(\text{the number of incident photons})\} \times 100 \quad (1)$$

The number of reacted electrons was determined from the amount of evolved H_2. The number of incident photons was determined by a chemical actinometry employing ammonium ferrioxalate and a photodiode (OPHIR: PD300-UV of a head and NOVA of a power monitor).

Characterization of Photocatalysts. Diffuse reflection spectra were obtained using a UV−vis−NIR spectrometer (Jasco; UbestV-570) and were converted from reflection to absorbance by the Kubelka−Munk method. Surface areas were determined by BET measurement (Coulter; SA3100). Photocatalyst powders were observed by a scanning electron microscope (Hitachi; S-5000) or transmittance electron microscopes (Hitachi; H-9000 and JEOL; JEM-2000F). X-ray absorption spectra of NiO-loaded photocatalysts at Ni K-edge were obtained at the BL9A facility of the Photon Factory in the Institute of Materials Structure Science, High Energy Accelerator Research Organization (KEK−IMSS−PF) in Tsukuba. The electron energy and currents for the storage ring were 2.5 GeV and 450−300 mA, respectively. High-intensity white X-rays emitted from the storage ring were monochromatized using a Si(111) double crystal monochromator. Before and after the monochromator, collimation and focusing mirrors were installed, respectively. The critical energy of both mirrors was set at 15 keV which was lower than the third-order higher harmonics of Si(111) in the Ni K-edge region. Five-tenths gram of a NiO-loaded photocatalyst was mixed with 0.2 g of boron nitride (Wako pure Chemical; 99.5%). The mixture was pressed into a disk. X-ray absorption spectra of NiO-loaded photocatalysts were obtained in the fluorescent mode using a Lytle detector whereas those of NiO and a Ni foil of reference samples were obtained in a transmittance mode. The EXAFS data were analyzed by the EXAFS analysis program REX version 2.5. Background was subtracted and k^3-weighted EXAFS oscillation was Fourier transformed over 3−12 $Å^{-1}$. The curve fitting analyses were carried out using an empirically derived phase shift and amplitude functions from NiO.

Results and Discussion

Photocatalytic Activities of $NaTaO_3$ Doped with Lanthanum for Water Splitting. Table 1 shows photocatalytic activities of $NaTaO_3$ doped with various amounts of lanthanum. Nondoped $NaTaO_3$ with and without a NiO cocatalyst was active as reported previously.[14e] The lanthanum doping improved the photocatalytic activity. In the naked $NaTaO_3$:La, the highest activity was obtained when 1 mol % of lanthanum was doped. As the amount of doped lanthanum was larger, the activity was decreased. The activity of $NaTaO_3$:La(10%) was lower than that

(14) (a) Kudo, A.; Kato, H. *Chem. Lett.* **1997**, 867−868. (b) Kato, H.; Kudo, A. *Chem. Phys. Lett.* **1998**, *295*, 487−492. (c) Kato, H.; Kudo, A. *Chem. Lett.* **1999**, 1207−1208. (d) Kudo, A.; Okutomi, H.; Kato, H. *Chem. Lett.* **2000**, 1212−1213. (e) Kato, H.; Kudo, A. *J. Phys. Chem. B* **2001**, *105*, 4285−4292. (f) Kato, H.; Kudo, A. *J. Photochem. Photobiol., A* **2001**, *145*, 129−133.
(15) Ishihara, T.; Nishiguchi, H.; Fukamachi, K.; Takita, Y. *J. Phys. Chem. B* **1999**, *103*, 1−3.
(16) Machida, M.; Yabunaka, J.; Kijima, T. *Chem. Mater.* **2000**, *12*, 812−817.
(17) Kudo, A.; Kato, H. *Chem. Phys. Lett.* **2000**, *331*, 373−377.

Table 1. Photocatalytic Activities of $NaTaO_3$:La for Water Splitting[a]

amount of La doped/mol %	band gap/eV	surface area/$m^2\ g^{-1}$	amount of NiO loaded/wt %	activity/mmol h^{-1}	
				H_2	O_2
none	4.00	0.44	none	0.17	0.08
			0.05	2.18	1.10
1	4.09	2.5	none	0.57	0.27
			0.2	12.1	5.77
2	4.09	3.2	none	0.45	0.21
			0.2	19.8	9.66
			2.0	2.65	1.37
3	4.09	3.4	none	0.31	0.15
			0.2	16.8	8.05
5	4.09	3.2	none	0.21	0.10
			0.2	9.96	4.79
10	4.09	3.2	none	0.12	0.06
			0.2	0.62	0.30

[a] Catalyst: 1 g, pure water: 390 mL, inner irradiation cell made of quartz, 400 W high-pressure mercury lamp.

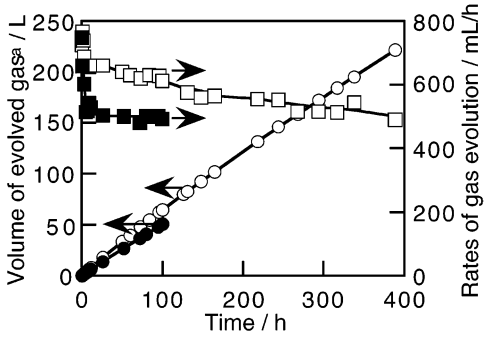

Figure 1. Photocatalytic water splitting over NiO(0.2 wt %)/$NaTaO_3$:La-(2%) in pure water (closed marks) and 1 mmol L^{-1} of an aqueous NaOH solution (open marks). (a) The amounts of evolved gas were determined by volumetric measurement. Catalyst: 1.0 g, reactant solution: 390 mL, inner irradiation cell made of quartz, 400 W high-pressure mercury lamp.

of nondoped $NaTaO_3$. The photocatalytic activities of $NaTaO_3$:La except for $NaTaO_3$:La(10%) were increased by 20−50 times when NiO cocatalysts were loaded. Among NiO/$NaTaO_3$:La photocatalysts, NiO/$NaTaO_3$:La(2%) showed the highest activity. The rates of H_2 and O_2 evolution over this catalyst were 19.8 and 9.7 mmol h^{-1}, respectively. The activity of NiO/$NaTaO_3$:La(10%) was smaller than NiO/$NaTaO_3$ as well as the case of the naked photocatalyst. A surface area of $NaTaO_3$:La-(1%) powder was 2.5 $m^2\ g^{-1}$, while those of $NaTaO_3$:La(2−10%) powder were about 3.3 $m^2\ g^{-1}$. Therefore, the surface area was not an important factor for water splitting on the present photocatalyst system as usual. Band gaps of $NaTaO_3$:La were 0.09 eV larger than that of nondoped $NaTaO_3$. It was considered that the conduction band levels of $NaTaO_3$:La shifted to negative, more or less, even if the increase in the band gaps would be due to changes in the potentials of both valence and conduction bands. The negative shifts of the conduction bands might be one of the factors for the improvement in the photocatalytic activities by doping of lanthanum.

Figure 1 shows long run experiments for the highly efficient photocatalytic water splitting over the optimized NiO(0.2 wt %)/$NaTaO_3$:La(2%) photocatalyst in pure water and an aqueous NaOH solution (1 mmol L^{-1}). In these cases, amounts of evolved gas (a mixture of H_2 and O_2) were determined by the volumetric measurement because of the high activity. The gas evolved in the rate of 750 mL h^{-1} (H_2: 500 mL h^{-1} and O_2: 250 mL h^{-1}) from pure water and an aqueous NaOH solution at the initial stages. These rates corresponded to 1.1 A of the current for H_2 and O_2 evolution by an electrolysis of water. This value strongly indicated how the photocatalytic water splitting efficiently proceeded over the NiO/$NaTaO_3$:La photocatalyst.

The deactivation was suppressed in an aqueous NaOH solution more than in pure water. Two hundred twenty liters of gas evolved after 390 h irradiation. The similar effect of the addition of a small amount of NaOH was also observed in NiO/$NaTaO_3$.[14e] The elution and redeposition of the nickel species were suppressed by the addition of NaOH, resulting in the suppression of deactivation. In NiO/$NaTaO_3$:La, it was considered that the addition of a small amount of NaOH stabilized the loaded NiO cocatalyst. In addition, the elution of sodium ions from the surface which might also cause the deactivation was suppressed by addition of NaOH into the reactant solution. The apparent quantum yields using 0.5, 0.1, and 0.05 g of photocatalyst powders and the monochromatic photon flux (300 μmol h^{-1}) were 29, 38, and 56%, respectively. Thus, it has been found that NiO/$NaTaO_3$:La is a highly efficient photocatalyst with good stability. The apparent quantum yields depended on the amount of the photocatalyst in the present system. When a large amount of photocatalyst powder is suspended, the photocatalyst particles were alternately irradiated because the incident light is absorbed by some of photocatalyst particles which post in the upper side (direction to the light source) of suspension. In contrast, photocatalyst particles were continuously irradiated in the diluted suspension. In the NiO/$NaTaO_3$:La system, the continuous irradiation to each photocatalyst particle seems to be necessary to obtain the high apparent quantum yield. An induction period is probably necessary, for example, for accumulation of photogenerated carriers, once photocatalyst particles are shut out from the irradiation. Moreover, the dependence of the apparent quantum yield upon the amount of photocatalyst may also suggest that the quantum yield depends on the light intensity per photocatalyst particle, which also affects the accumulation of photogenerated carriers.

Realization of highly efficient water splitting had been thought to be questionable in a period in which TiO_2 powder photocatalysts had extensively been studied for water splitting. The present study was able to demonstrate that the highly efficient photocatalytic water splitting was actually possible using a photocatalyst powder system.

The photocatalytic activities for H_2 and O_2 evolution from aqueous solutions of methanol and silver nitrate were also investigated to clarify which of H_2 or O_2 evolution was enhanced by doping of lanthanum (Table 2). The activity of native $NaTaO_3$:La(2%) for H_2 evolution (run 5) was only 30% higher than that of nondoped $NaTaO_3$ (run 1) while the activity of $NaTaO_3$:La(2%) for O_2 evolution (run 6) was 2 times higher than that of nondoped $NaTaO_3$ (run 2). The results suggested that doping of lanthanum improved O_2 evolution more than H_2 evolution by creating O_2 evolution sites. However, the activity of NiO/$NaTaO_3$:La(2%) for O_2 evolution from an aqueous silver nitrate solution (Run 8) was lower than that from pure water (Table 1). It was due to the shield of the incident light and the blocking of active sites by deposited metallic silver. On the other hand, the effect of loading of the NiO cocatalyst on H_2 evolution was much larger for $NaTaO_3$:La (runs 5 and 7) than nondoped $NaTaO_3$ (runs 1 and 3). The activity of NiO/$NaTaO_3$:La(2%)

Table 2. Photocatalytic H_2 and O_2 Evolution from Aqueous Solutions Containing Sacrificial Reagents over $NaTaO_3$ and $NaTaO_3$:La(2%) Photocatalysts[a]

run	catalyst	cocatalyst	Sacrificial reagent	activity/mmol h^{-1} H_2	O_2
1	$NaTaO_3$	none	CH_3OH[b]	10.3	
2		none	$AgNO_3$[c]		0.78
3		NiO(0.05 wt %)	CH_3OH[b]	16.8	
4		NiO(0.05 wt %)	$AgNO_3$[c]		0.86
5	$NaTaO_3$:La(2%)	none	CH_3OH[b]	13.2	
6		none	$AgNO_3$[c]		1.7
7		NiO(0.2 wt %)	CH_3OH[b]	38.4	
8		NiO(0.2 wt %)	$AgNO_3$[c]		1.7
9		Pt(1 wt %)	CH_3OH[b]	36.7	

[a] Catalyst: 1 g, reactant solution: 390 mL, inner irradiation cell made of quartz, 400 W high-pressure mercury lamp. [b] 10 vol % of an aqueous solution. [c] 0.05 mol L^{-1} of an aqueous solution.

for H_2 evolution was the same as that of $NaTaO_3$:La(2%) loaded with Pt of the most effective cocatalyst for H_2 evolution (run 9). It is well-known that NiO loaded on photocatalysts works as active sites for H_2 formation.[6,7,10,11] The photogenerated holes in valance bands consisting of O2p orbitals, of which potentials are ca. 3 V versus NHE,[18] should possess enough potential to form O_2 indicating the unnecessariness of cocatalysts. On the other hand, the present authors have reported photocatalytic reduction of nitrate ions over tantalates.[19] The selectivities for reduction products were changed by loading of NiO. Although the formation of nitrite ions was dominant over the naked tantalate photocatalyst, the selectivity for H_2 formation was especially increased by loading of NiO. In contrast, the NiO loading did not affect O_2 evolution (runs 6 and 8). These results suggested that the NiO cocatalyst loaded on the $NaTaO_3$:La powder possessed a specific state with an efficient H_2 evolution ability.

Characterization of $NaTaO_3$:La Crystals. The characterization of $NaTaO_3$:La crystals was carried out to clarify the factors of the increase in the photocatalytic activity by doping of lanthanum.

X-ray diffraction patterns of $NaTaO_3$:La powders were slightly shifted to lower angles as the amount of doped lanthanum was increased as shown in Figure 2. The shift indicated that a part of lanthanum at least was homogeneously doped into the $NaTaO_3$ lattice although the majority of lanthanum was localized near the surface. Ionic radii of 12-coordinated La^{3+} (1.36 Å) and Na^+ (1.39 Å) ions are almost the same as each other.[20] In contrast, an ionic radius of the six-coordinated La^{3+} ion (1.032 Å) is remarkably larger than that of the Ta^{5+} ion (0.64 Å).[20] If Ta^{5+} ions which were at the position of B sites in perovskite structures were replaced with La^{3+} ions, a large shift should be observed. Moreover, the diffraction pattern of $La_{0.33}TaO_3$ (the occupation factor of the A site is 0.33) with the perovskite structure similar to $NaTaO_3$ was observed at a lower angle than that of $NaTaO_3$.[21] Therefore, the small shifts to lower angles observed in the diffraction patterns of $NaTaO_3$:La suggested the substitution of lanthanum ions for sodium ions in the bulk which occupied A sites in perovskite structures.

$NaTaO_3$:La powders were observed by electron microscopes. Figure 3 shows the SEM images of nondoped $NaTaO_3$ and

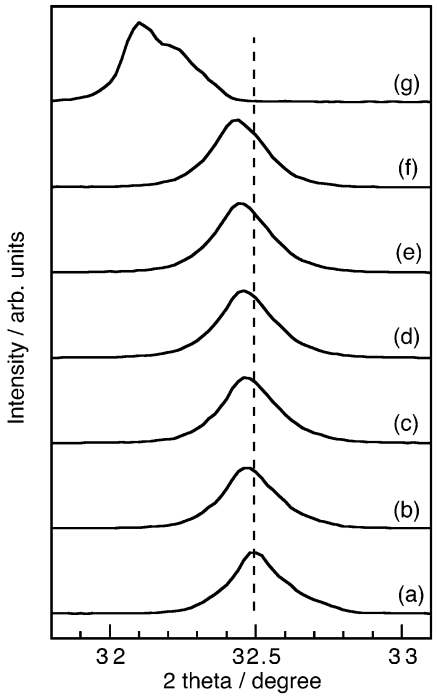

Figure 2. X-ray diffraction peaks around 32.5° of (a) nondoped $NaTaO_3$ and $NaTaO_3$ doped with lanthanum; (b) 1%, (c) 2%, (d) 3%, (e) 5%, and (f) 10%, and (g) $La_{0.33}TaO_3$.

$NaTaO_3$:La(2%) powders prepared by the same conditions. Both particles were well-crystallized. The particle size of $NaTaO_3$:La powder, 0.1−0.7 μm, was remarkably smaller than that of nondoped $NaTaO_3$ powder, 2−3 μm. Ordered surface nanostep structure was observed for the La-doped $NaTaO_3$ powder whereas the surface of nondoped $NaTaO_3$ was flat. The decrease in the particle size and the creation of the nanostep structure were also observed for other lanthanum-doped $NaTaO_3$ photocatalysts listed in Table 1.

Figure 4a shows the TEM image of a $NaTaO_3$:La(5%) crystal. The steps with 3−15 nm of the height were observed as seen in a SEM image. The ordered surface nanostructure was self-constructed. The clear fringes indicated the high crystallinity of $NaTaO_3$:La. The small particle with the high crystallinity is advantageous for the photocatalytic activity. In the previous paper, the authors have reported that the addition of the excess amount of sodium in the $NaTaO_3$ preparation suppressed formation of sodium ion defects in $NaTaO_3$ crystals, resulting in the drastic improvement of photocatalytic activity.[14e] In the nondoped $NaTaO_3$, the increase in the crystal size by addition of the excess amount sodium was not advantageous. In contrast, in the La-doped $NaTaO_3$, it was revealed by the SEM and TEM observation that doping of lanthanum made the crystal size small with the high crystallinity. Thus, doping of lanthanum let $NaTaO_3$ crystal possess the two advantageous factors, the high crystallinity and the small crystal size; it was impossible for nondoped $NaTaO_3$. These were factors for the drastic improvement in the photocatalytic activity by doping of lanthanum.

Energy-dispersive X-ray spectra for the edge and the groove of the step structure and the bulk (corresponding to the points A, B, and C indicated in Figure 4a, respectively) were measured by TEM-EDS as shown in Figure 4b. Lanthanum Lα lines were observed at the edge and the groove of the step structure whereas it was not detected in the bulk. The relative peak intensity of a

(18) Scaife, D. E. *Solar Energy* **1980**, *25*, 41−54.
(19) Kato, H.; Kudo, A. *Phys. Chem. Chem. Phys.* **2002**, *4*, 2833−2838.
(20) Shannon, R. D. *Acta Crystallogr.* **1976**, *A32*, 751−767.
(21) Iyer, P. N.; Smith, A. J. *Acta Crystallogr.* **1967**, *23*, 740−746.

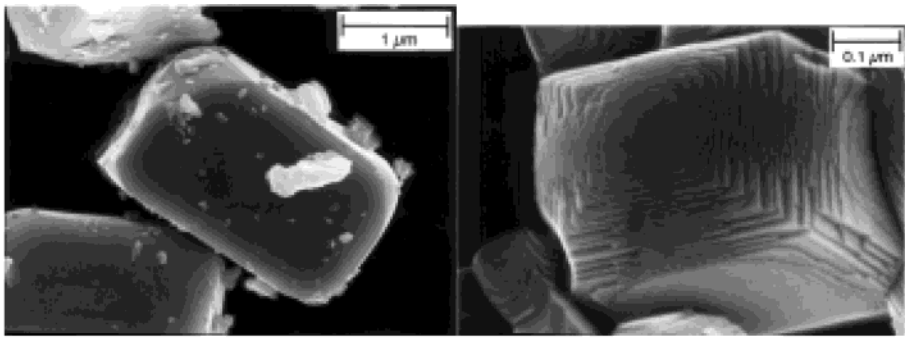

Figure 3. Scanning electron microscope images of (a) nondoped $NaTaO_3$ and (b) $NaTaO_3$:La(2%).

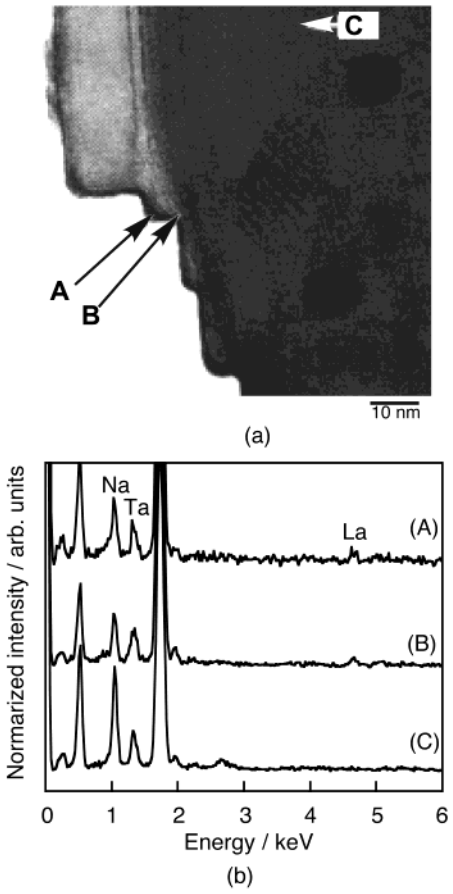

Figure 4. (a) Transmittance electron microscope image of $NaTaO_3$:La-(5%). (b) Energy-dispersive X-ray spectra of $NaTaO_3$:La(5%) at (A) the edge, (B) the groove of the step structure, and (C) the bulk, corresponding to points A, B, and C in the TEM image, respectively.

Na Kα line at 1 keV to a Ta Mζ line at 1.3 keV for the edge and the groove of the step structure was smaller than that for the bulk. The results revealed that the majority of doped lanthanum localized near the surface and was substituted for sodium ions as well as in the bulk. The substitution of La^{3+} ions for Na^{+} ions may increase the n-type property of $NaTaO_3$ resulting in the increase in the electric conductivity. It would be one of the factors for the enhancement of photocatalytic activity by doping of lanthanum. The substitution with a heavy element of lanthanum near the surface might cause the dark contrast at the edge of the crystal observed in the TEM image as shown in Figure 4a. It was considered from the results that

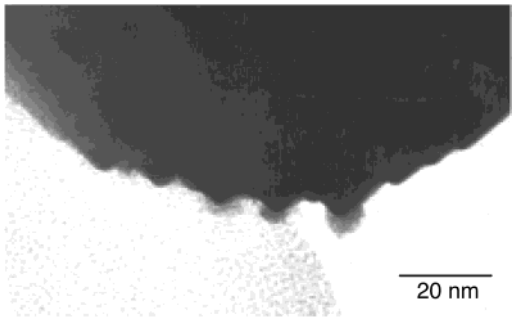

Figure 5. Transmittance electron microscope image of NiO(0.5 wt %)/ $NaTaO_3$:La(1.5%).

the lanthanum localizing near the surface prevented the crystal growth, resulting in the formation of fine particles and the creation of the characteristic nanoscale step structure. These effects of doping of lanthanum were also observed for all lanthanum-doped $NaTaO_3$ being independent of the amount of doped lanthanum. However, localization of lanthanum near the surface suggested that the surface active sites would be collapsed when a large amount of lanthanum was doped. The decrease in the photocatalytic activity by the large amount of lanthanum doping was due to this negative effect of lanthanum doping. On the other hand, the diffraction peaks not assigned to $NaTaO_3$ were observed for $NaTaO_3$:La(10%) in the XRD measurement, indicating the formation of the impurity phase or the distortion of the lattice. The interface between $NaTaO_3$:La and the impurity phase may act as recombination centers between photogenerated electrons and holes resulting in the decrease in the photocatalytic activity. However, the diffraction peaks had not been assigned to Ta-, La-, Na−Ta-, La−Ta-, Na−La−Ta-, and Na−La-oxides. On the other hand, the lattice distortion would also lower the activity of $NaTaO_3$:La(10%).

Characterization of NiO Cocatalysts Loaded on $NaTaO_3$:La Photocatalysts—Determination of H_2 Evolution Sites. It was suggested that NiO cocatalysts were loaded on $NaTaO_3$:La as a specific state with an efficient H_2 evolution ability as mentioned above. NiO(0.5 wt %)/$NaTaO_3$:La(1.5%) was observed by TEM as shown in Figure 5. Spherical NiO particles (3−8 nm) were selectively loaded on the edges of the nanostep structure. In NiO(0.2 wt %)/$NaTaO_3$ not doped with lanthanum, many islands of NiO particles (10−20 nm) were observed by SEM.[14e] However, NiO particles were rarely observed by TEM in the present NiO(0.5 wt %)/$NaTaO_3$:La photocatalyst even if

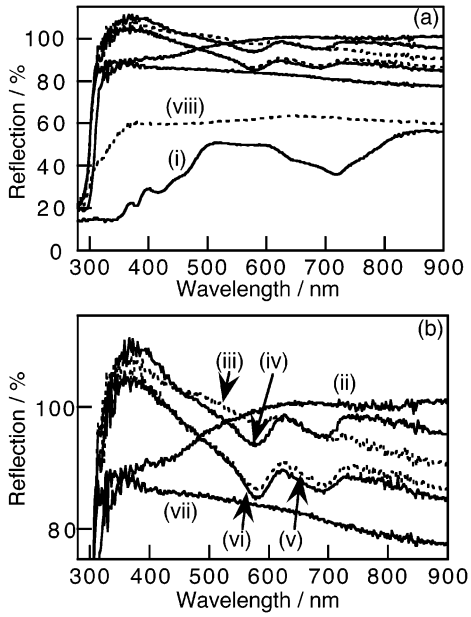

Figure 6. (a) Diffuse reflection spectra of (i) NiO, (ii) NiO(0.05 wt %)/$NaTaO_3$, NiO(0.2 wt %)/$NaTaO_3$:La ((iii) 1%, (iv) 2%, (v) 3%, (vi) 5%, and (vii) 10%), and (viii) NiO(2 wt %)/$NaTaO_3$:La(2%) and (b) shows the magnification of (a).

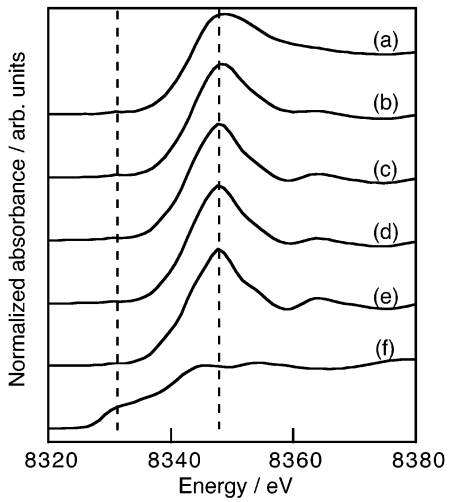

Figure 7. X-ray absorption near-edge structure (XANES) spectra of $NaTaO_3$:La(1.5%) loaded with NiO ((a) 0.2 wt %, (b) 0.5 wt %, (c) 2 wt %), (d) nondoped $NaTaO_3$ loaded with NiO(0.2 wt %), (e) NiO, and (f) Ni foil.

the amount of NiO was larger than that of NiO(0.2 wt %)/$NaTaO_3$. A large number of NiO particles with sizes large enough to be observed by TEM should have been observed taking the amount of loaded NiO into account even if the NiO particles are amorphous. In addition, the photocatalytic activity was drastically improved by loading of NiO although most of the $NaTaO_3$:La crystals were not loaded as observable NiO particles. These results indicated that ultrafine NiO particles with smaller sizes than the resolution of TEM should exist. On the other hand, the large NiO particles were deposited on the edges of the surface nanostep structure, implying that ultrafine NiO particles would also be selectively deposited on the edges.

The colors of NiO-loaded $NaTaO_3$:La(1−5%) were pale violet, whereas that of NiO-loaded $NaTaO_3$ was light gray as well as usual NiO-loaded photocatalysts. It also suggested that the characteristic of NiO cocatalysts loaded on $NaTaO_3$:La was different from that of the usually loaded NiO cocatalyst. Figure 6 shows diffuse reflection spectra of NiO-loaded $NaTaO_3$:La and $NaTaO_3$. NiO/$NaTaO_3$:La with 1−5 mol % of lanthanum showed characteristic absorption bands at 580 and 690 nm being different from the bulky green NiO and usual grayish loaded NiO. As far as the authors know, there are no reports for the NiO particle possessing absorption bands at 580 and 690 nm. The loaded nickel may complex with sodium, lanthanum, and tantalum. Three reference materials, $NaTaO_3$ loaded with both nickel and lanthanum, $NaTaO_3$ doped with Ni^{2+}, and $NiTa_2O_6$, were prepared to investigate the absorption property. However, the characteristic absorption bands were not observed. Therefore, the characteristic absorption bands seem to be due to the ultrafine NiO particle which may interact with the surface. On the other hand, the photocatalytic activities of NiO/$NaTaO_3$:La(1−5%) depended on the amount of lanthanum doping (Table 1); even the loaded NiO showed the similar characteristic absorption bands. It was due to the photocatalytic ability of native $NaTaO_3$:La and depended on the amount of lanthanum as mentioned above. Moreover, such characteristic absorption bands were not observed for NiO(0.2 wt %)/$NaTaO_3$:La(10%) and NiO(2 wt %)/$NaTaO_3$:La(2%) of which photocatalytic activities were not high as shown in Table 1. The results suggested that the specific state of NiO cocatalysts with the characteristic absorption bands contributed to the formation of highly active sites for H_2 evolution.

Figures 7 and 8 show Ni K-edge X-ray absorption near-edge structure (XANES) spectra and the Fourier transforms of k^3-weighted EXAFS oscillation for NiO/$NaTaO_3$:La(1.5%) with various amounts of NiO, respectively. The curve fitting analyses of EXAFS data for Ni K-edge of NiO/$NaTaO_3$:La photocatalysts are summarized in Table 3. The XANES spectra of all NiO/$NaTaO_3$:La were similar to that of the bulk NiO. No existence of the metallic Ni was also confirmed from EXAFS spectra. In the EXAFS spectrum of NiO(0.2 wt %)/$NaTaO_3$:La(1.5%) with the highest activity, the contribution of long-distance shells (3−5 Å) was hardly observed (Figure 8a). Moreover, the magnitude of the Ni−Ni (oxide) shell was small in comparison with that of the Ni−O shell. When 0.5 wt % of NiO was loaded, the contribution of higher shells was observed in the EXAFS spectrum, however, the contribution to the spectrum and the coordination number were still very small (Figure 8b, Table 3). EXAFS data of loaded NiO can be different from those of bulk NiO if the loaded NiO is an ultrafine particle, a mix-oxide, an amorphous phase, and moreover distorted or substituted in the $NaTaO_3$ lattice. The $NaTaO_3$ loaded with both nickel and lanthanum did not show the characteristic absorption bands observed for NiO(0.2 wt %)/$NaTaO_3$:La(1−5%), as described above. The substitution of nickel in the $NaTaO_3$ lattice seems to be impossible at the calcination temperature of NiO/$NaTaO_3$:La (540 K). In addition, Ni^{2+}-doped $NaTaO_3$ also did not show the characteristic absorption bands. No large amorphous NiO particles were observed by TEM as mentioned above. If the change in EXAFS data were due to not the formation of ultrafine particles but the distortion of the NiO lattice, a large number of NiO particles should be observed by TEM. However, only few NiO particles were observed for NiO(0.5 wt %)/$NaTaO_3$:La as described above. Therefore, EXAFS results indicated that the majority of NiO were loaded as highly dispersed ultrafine particles without long-range ordering in the cases of small

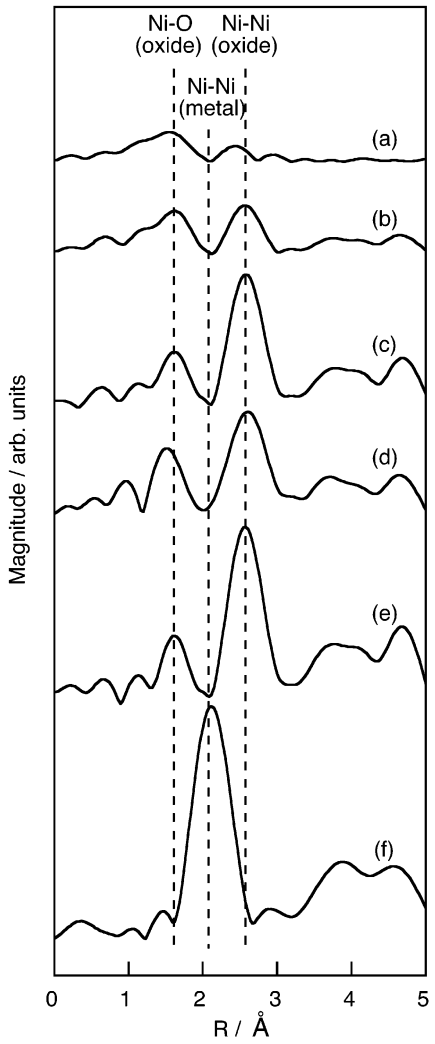

Figure 8. Fourier transforms of k^3-weighted EXAFS oscillation for $NaTaO_3$:La(1.5%) loaded with NiO ((a) 0.2 wt %, (b) 0.5 wt %, (c) 2 wt %), (d) nondoped $NaTaO_3$ loaded with NiO(0.2 wt %), (e) NiO, and (f) Ni foil.

Table 3. Curve Fitting Analysis of EXAFS Data for Ni K-edge of $NiO/NaTaO_3$:La Photocatalysts

	Ni–O		Ni–Ni	
catalyst	N	*r*/Å	N	*r*/Å
NiO	6	2.09	12	2.95
NiO(0.2 wt %)/$NaTaO_3$:La(1.5%)	3	2.01	1	2.81
NiO(0.5 wt %)/$NaTaO_3$:La(1.5%)	4.4	2.07	3.5	2.95
NiO(2 wt %)/$NaTaO_3$:La(1.5%)	5.8	2.08	10.5	2.95
NiO(0.2 wt %)/$NaTaO_3$	5.7	2.05	8.4	2.95

amounts of NiO loading (~0.5 wt %). The contribution of long-distance shells in NiO(0.5 wt %)/$NaTaO_3$:La(1.5%) was probably due to a few large NiO particles observed by TEM as shown in Figure 5. NiO(2 wt %)/$NaTaO_3$:La(1.5%) showed the similar EXAFS spectrum to that of bulk NiO of a reference sample (Figure 8c). On the other hand, NiO was also loaded as the bulky NiO on nondoped $NaTaO_3$ (Figure 8d). Thus, the ultrafine NiO particles were obtained only in the cases of loading of the small amounts of NiO on $NaTaO_3$:La with the nanostep structure. No remarkable difference in the EXAFS spectra of NiO(0.2 wt %)/$NaTaO_3$:La(1.5%) was observed between before and after a photocatalytic water splitting reaction. It indicated

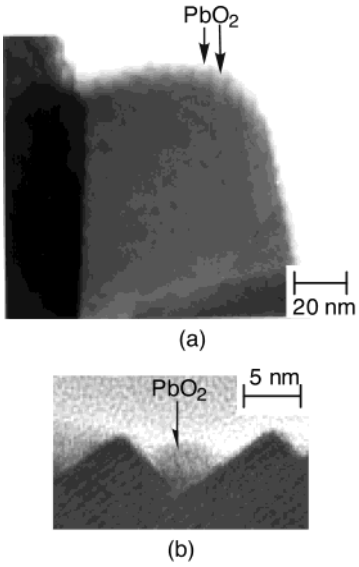

Figure 9. (a) Transmittance electron microscope image of $NaTaO_3$:La(2%) with photodeposited PbO_2 (3.5 wt %). (b) PbO_2 particles deposited on the groove of the nanostep structure selectively.

that the ultrafine NiO particles were stable for photocatalytic water splitting.

The results of photocatalytic activities, TEM, DRS, and EXAFS led to the conclusion that the majority of NiO was loaded as ultrafine particles in the cases of NiO/$NaTaO_3$:La when the amounts of NiO loading were small (~0.5 wt %), and it was one of the important factors for highly efficient photocatalytic water splitting in the present NiO/$NaTaO_3$:La system. The NiO cluster which interacts with the $NaTaO_3$ surface can be imagined for the state of the ultrafine NiO particle, it may be regarded as a surface complex in the extreme case. The formation of the clusterlike ultrafine NiO particles was due to the specific sites, in which lanthanum ions were located near the surface and the electronic state was changed by the substitution of lanthanum ions for sodium ions, formed at the nanostep structure created by doping of lanthanum.

Determination of O_2 Evolution Sites. It was found from TEM observation that NiO cocatalysts tended to be loaded on the edges at the nanostep structure. Moreover, EXAFS analyses revealed that the loaded NiO was ultrafine particles. Such a specific NiO worked as the efficient cocatalyst for H_2 evolution as well as Pt as shown in Table 2. On the other hand, the activity for O_2 evolution from an aqueous silver nitrate solution was increased by 2 times when lanthanum was doped as shown in Table 2. The results suggested that active sites for O_2 evolution were created by doping of lanthanum as mentioned previously. It has been reported that PbO_2 particles are oxidatively photodeposited on oxidation sites[22] as follows:

$$Pb^{2+} + 2h^+ + 2H_2O \rightarrow PbO_2 + 4H^+ \qquad (2)$$

Therefore, PbO_2 photodeposited on the $NaTaO_3$:La powder was observed by TEM to obtain the information for the reaction site as shown in Figure 9a. PbO_2 particles were deposited on the flat surfaces and the nanostep structures. At the nanostep structure, PbO_2 particles were mainly deposited not on the edges

(22) Matsumoto, Y.; Noguchi, M.; Matsunaga, T. *J. Phys. Chem. B* **1999**, *103*, 7190−7194.

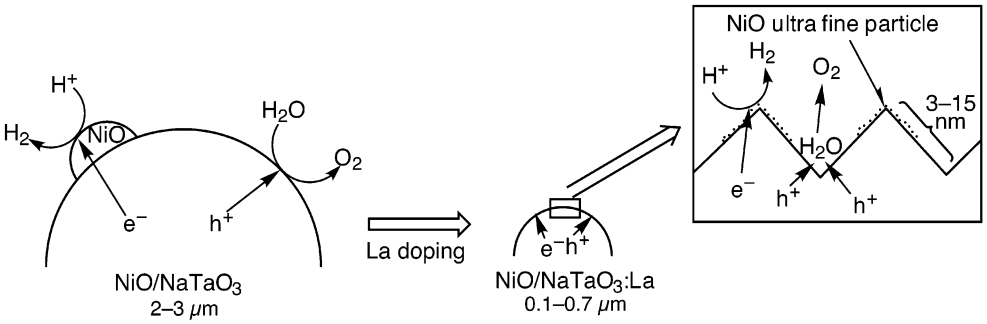

Figure 10. Mechanism of highly efficient photocatalytic water splitting over $NiO/NaTaO_3$:La photocatalysts.

but on the grooves selectively and orderly as shown in Figure 9b. The results indicated that the oxidation sites existed at the flat surfaces and the grooves of the nanostep structure. The oxidation sites on the flat surfaces of $NaTaO_3$:La would possess the similar ability to those of nondoped $NaTaO_3$. Therefore, the increase in the activity for O_2 evolution by doping of lanthanum was due to the creation of efficient sites at the grooves in the surface nanostep structure.

Mechanism of Highly Efficient Water Splitting over $NiO/NaTaO_3$:La Photocatalysts. The mechanism of highly efficient water splitting over $NiO/NaTaO_3$:La photocatalysts is illustrated in Figure 10. Photogenerated electrons and holes have to migrate in a long distance to the surface active sites in nondoped $NaTaO_3$ photocatalysts with a large particle size. Fine $NaTaO_3$ particles with a high crystallinity were obtained by doping of lanthanum. In the $NaTaO_3$:La powder, photogenerated electrons and holes do not have to migrate in so long a distance because of the small particle size. As the particle size is decreased, the probability of the surface reaction of electrons and holes with water molecules is increased in comparison with that of the recombination in the bulk. Moreover, the characteristic nanostep structure was created at the surface of the $NaTaO_3$:La crystal. The reaction sites for H_2 and O_2 evolution were effectively separated from each other at the characteristic nanostep structure. At the edges of the reduction sites, water can be efficiently reduced to H_2 on the highly dispersed ultrafine NiO particles. On the other hand, the grooves of the nanostep structure provide the catalytic active sites for O_2 formation accompanied with four-electrons oxidation and the coupling of oxidized intermediate species. The mechanism for the efficient O_2 evolution at the grooves in the nanostep structure was considered as follows. The photogenerated holes migrated to the groove of oxidation sites. Geometry of the walls on both sides of the groove would facilitate the multihole injection and the coupling between intermediate species to form O_2. Thus, O_2 formation can be promoted by the geometric effects at the groove of the nanostep structure. As mentioned above, the small particle size and the ordered surface nanostep structure created by the lanthanum doping contributed to suppression of recombination between photogenerated electrons and holes and the separation of active sites to avoid the back reaction, resulting in the highly efficient water splitting into H_2 and O_2.

Conclusions

(1) The photocatalytic activity of $NiO/NaTaO_3$ was remarkably increased by doping of lanthanoids ions. The optimized NiO(0.2 wt %)/$NaTaO_3$:La(2%) photocatalyst showed the high activity for water splitting into H_2 and O_2. H_2 and O_2 evolved with rates of 19.8 and 9.7 mmol h^{-1}, respectively. The maximum apparent quantum yield of the $NiO/NaTaO_3$:La photocatalyst was 56% at 270 nm. The activity was stable for more than 400 h.

(2) The factors for the high activity of the $NiO/NaTaO_3$:La photocatalyst were clarified by characterization. Fine $NaTaO_3$ particles with high crystallinity were obtained by doping of lanthanum. As the particle size is decreased, the probability of the surface reaction of electrons and holes with water molecules is increased in comparison with recombination in the bulk. Moreover, the characteristic nanostep structure was created at the surface of the $NaTaO_3$:La crystal. The reaction sites were effectively separated at the step structure as the edges for the reduction sites and the grooves for the oxidation sites. In the $NiO/NaTaO_3$:La photocatalysts with the high activities, NiO cocatalysts were loaded as ultrafine NiO particles possessing characteristic absorption bands at 580 and 690 nm. The ultrafine NiO particles were highly active for H_2 formation as well as Pt of an excellent cocatalyst. On the other hand, at the grooves of the oxidation sites, the geometric effects would enhance the O_2 formation accompanied with four-electrons oxidation and the complex molecular combination. These factors affect the highly efficient photocatalytic water splitting over $NiO/NaTaO_3$:La photocatalysts.

Acknowledgment. X-ray absorption measurement was carried out under the approval of the Photon Factory Advisory Committee (Proposal No. 2001G110). This work was supported by Core Research for Evolutional Science and Technology (CREST) and Tokyo Ohka foundation for the Promotion of Science and Technology. One of us (H.K.) has been awarded a Research Fellowship of the Japan Society for the Promotion of Science for Young Scientists.

JA027751G